

Geology and Mineral Chemistry of Gold Mineralization in Mirge-Naqshineh Occurrence (Saqez, NW Iran): Implications for Transportation and Precipitation of Gold

Golale ASGHARI^{1,*}, Samad ALIPOUR¹, Hossein AZIZI² and Hassan MIRNEJAD³

¹ Department of Geology, Urmia University, Urmia, Iran

² Mining Department, Faculty of Engineering, University of Kurdistan, P.O. Box 416, Sanandaj, Iran

³ Department of Geology, Faculty of Science, University of Tehran, Tehran, Iran

Abstract: The Mirge-Naqshineh gold district is situated at northwest of Iran with a NW-trending brittle-ductile shear zone. It is hosted by Precambrian meta-sedimentary and meta-volcanic units traversed by mineralized quartz veins. In terms of cross-cutting relationships and sulfide content three types of quartz veins are identified in the region. Among those, parallel to bedding quartz vein (type I) is the main host for gold mineralization. Gold is found in three different forms: 1) submicrometer-size inclusions of gold in arsenian pyrite, 2) as electrum and 3) in the crystal lattice of sulfides (pyrite, galena and chalcopyrite). Six types of pyrite (Py1-Py6) were identified in this ore reserve. Py3 coexists with arsenopyrite and contains the greatest As-Au concentrations. There is a negative correlation between the As and S contents in Py2 and Py3, implying the substitution of sulfur by arsenic. Pyrites and mineralized quartz veins were formed via metamorphic-hydrothermal fluid and reflect the gold-transportation as $\text{Au}(\text{HS})_2$ under reducing and acidic conditions. The gold precipitation mainly controlled by crystallization of arsenian pyrite during fluid/rock interactions and variation of $f\text{O}_2$. The volcanic host rock has played an important role in gold concentration, as Py3 in this rock contains inclusion of gold particles, but gold is within the lattice of pyrite in phyllite or other units.

Key words: gold, quartz veins, mineral chemistry, EPMA, Mirge-Naqshineh, Iran

1 Introduction

The majority of gold deposits are classed as orogenic gold deposits, which means that they occur in active margins of the continents, as, for example, the Alpine-Himalaya belt. Iran is located in the Alpine-Himalayan orogenic belt and has high potentials for gold deposits (Ghorbani, 2013). The Sardasht-Saqez goldfield is the most prospective area for gold exploration in northwestern Iran, which is associated with brittle-ductile shear zones (Tajeddin, 2004). The Geological Survey of Iran (GSI) carried out a preliminary geochemical exploration program on the Sardasht-Saqez area, in the mid-1990s-and reported gold anomalies and associated hydrothermal alteration in several districts include Mirge-Naqshineh, Kasnazan, Zaveh-koh, Hamzeh-Qaranein, Kervian, Qolqoleh and Qabaqloujeh (inset of Fig. 1).

In 2006, the GSI carried out a percussion trenching and

diamond drilling program. Results to date indicate a probable reserve of about 5 million tonnes of ore or 16 tonnes of gold with a grade of 1 to 4 g/t Au in these deposits (Aliyari et al., 2012). Previous studies had shown that the Qolqoleh, Kervian, and Ghabaghlujeheh orogenic gold occurrences are hosted by NE-trending ductile shear zones and younger brittle fractures (Heidari, 2004; Aliyari, 2006).

The present study focuses on the Mirge-Naqshineh gold occurrence, based on detailed investigation of paragenesis and mineral chemistry of pyrite and sulfide minerals in the district. Studying the texture, paragenesis and trace element composition of pyrite can provide insight into the evolution of ore system (Thomas et al., 2011; Agangi et al., 2013; Cook et al., 2013; Velásquez et al., 2014; Yan et al., 2014; Wang and Zhu, 2015; Nie et al., 2017; Zhang et al., 2017; Nourian Ramsheh et al., 2014). Pyrite is the most common sulfide in hydrothermal gold deposits, and it generally develops throughout different stages of

* Corresponding author. E-mail: g.asghari@urmia.ac.ir

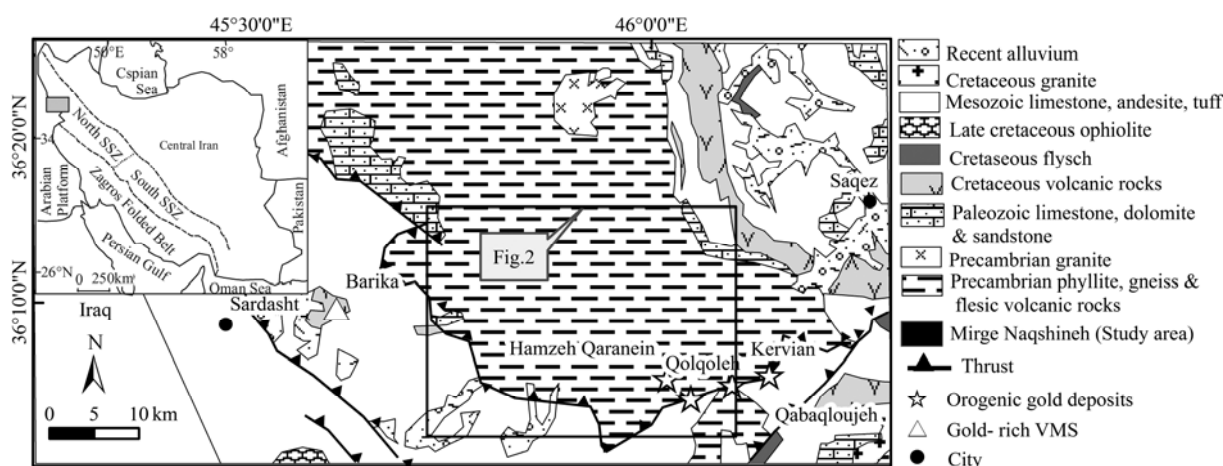


Fig. 1. Simplified geological map of tectonic subdivisions of Iran and Sardasht-Saqez area with distribution of gold deposits. SSZ – Sanandaj-Sirjan zone.

mineralization. Various vein types and pyrite generations are described to define the physical-chemical conditions of fluids associated with the hydrothermal and structural events in the Mirge-Naqshineh area. These results should lead to better understanding of the ore-forming and the physicochemical processes that affect ore transport and deposition, also can be effective in the exploration and processing techniques in the future of this area.

2 Geological Setting

2.1 Regional geology

The Mirge-Naqshineh occurrence is central part of the Sardasht-Saqez goldfield, located in the northern part of the Sanandaj-Sirjan metamorphic zone (SSZ) of Iran (Fig. 1). The SSZ formed by collision of the Afro-Arabian continent and Iranian microcontinent, and subsequent southward propagation of the fold-thrust belt, during Neo-Tethys subduction and the Cretaceous-Tertiary Zagros orogeny (Berberian and King, 1981; Alavi, 1994; Mohajjel and Fergusson, 2000; McQuarrie, 2004; Sarkarinejad and Azizi, 2008; Agard et al., 2005, 2011; Omrani et al., 2008).

The SSZ is subdivided into two parts: (1) The southeastern part comprises Paleozoic metamorphic rocks of relatively high metamorphic grade that were deformed and metamorphosed in the Middle to Late Triassic (Eftekharejad, 1981; Berberian, 1995), (2) The northwestern SSZ consists mostly of metasedimentary rocks (Baharifar et al., 2004) associated with widespread Mesozoic volcanic and intrusive felsic rocks (Fig. 1) which were affected by deformation in the Late Cretaceous (Eftekharejad, 1981; Ghasemi and Talbot, 2006).

In the northwestern part of the Sanandaj-Sirjan zone numerous granitoids are exposed within extensive realms

of sheared lower greenschist-facies rocks with Precambrian protolith ages (Eftekharejad, 1973). The resulting zircon U-Pb crystallization age for Sheikh Chupan granodiorite which is located in northeast of the study area (Fig. 2a) gives an age of 551 ± 25 Ma and field observations have indicated that granitoid does not intrude the sheared rocks and that it might represent the non-sheared equivalent of the greenschist protolith (Hassanzadeh et al., 2008).

The tectonic of the SSZ is characterized by numerous thrusts, all of which transport rock units to the southwest (Alavi, 1994), hosted gold deposits, spatially associated with first and second-order fault systems of major deep-seated faults (Mohajjel et al., 2003).

The Sardasht-Saqez thrust is marked by a series of syenitic to granitic mylonitized dikes and or sills, which are elongated parallel to the steeply dipping major reverse fault (approximately 100 km long, Fig. 1), and NE-trending goldfield belt hosted by mafic to intermediate meta-volcanic and meta-sedimentary rocks with Precambrian to Cretaceous age. Almost all the gold occurrences in the Sardasht-Saqez zone such as Mirge-Naqshineh formed in the greenschist-facies metamorphic rocks and located within or adjacent to the major deep Sardasht-Saqez fault and other confining normal faults across the metamorphic zone. They appear generally by controlled brittle structures within the ductile shear zones generated during Late Cretaceous-Tertiary (Aliyari et al., 2012).

2.2 Geology of the Mirge-Naqshineh area

The current understanding of geology of Mirge-Naqshineh, nearby town of Saqez (Fig. 1), is based on the combined result of extensive diamond drill-core logging (over 741 meter was logged in the course of this study) and field mapping. The Mirge-Naqshineh gold-bearing

district is embedded in the Precambrian basin (Omrani and Khabbaznia, 2003), predominantly consists of phyllite, slate, mica-schist and meta-sandstone with alternation of andesite and equivalent tuffs that intruded by small stocks of granite rocks (Fig. 2a and b).

Phyllite is carbonaceous and black with more than 100 m in thickness (Fig. 3). Schist units have variably dominated by sericite, quartz-muscovite and quartz-chlorite. Andesites are comprised of plagioclase

phenocrysts and alkali feldspar in a matrix rich in alkali feldspar and quartz. These rocks have undergone variable degrees of hydrothermal alteration, deformation and mylonitization and are cross-cut by quartz veins. Structurally, the Mirge-Naqshineh ore district is characterized by NW-SE-trending shear zone which extends for more than 800 m in length and 150 m in thickness and dips northeast at an angle of 20–55° (Fig. 2b). The average gold grade in this area has been

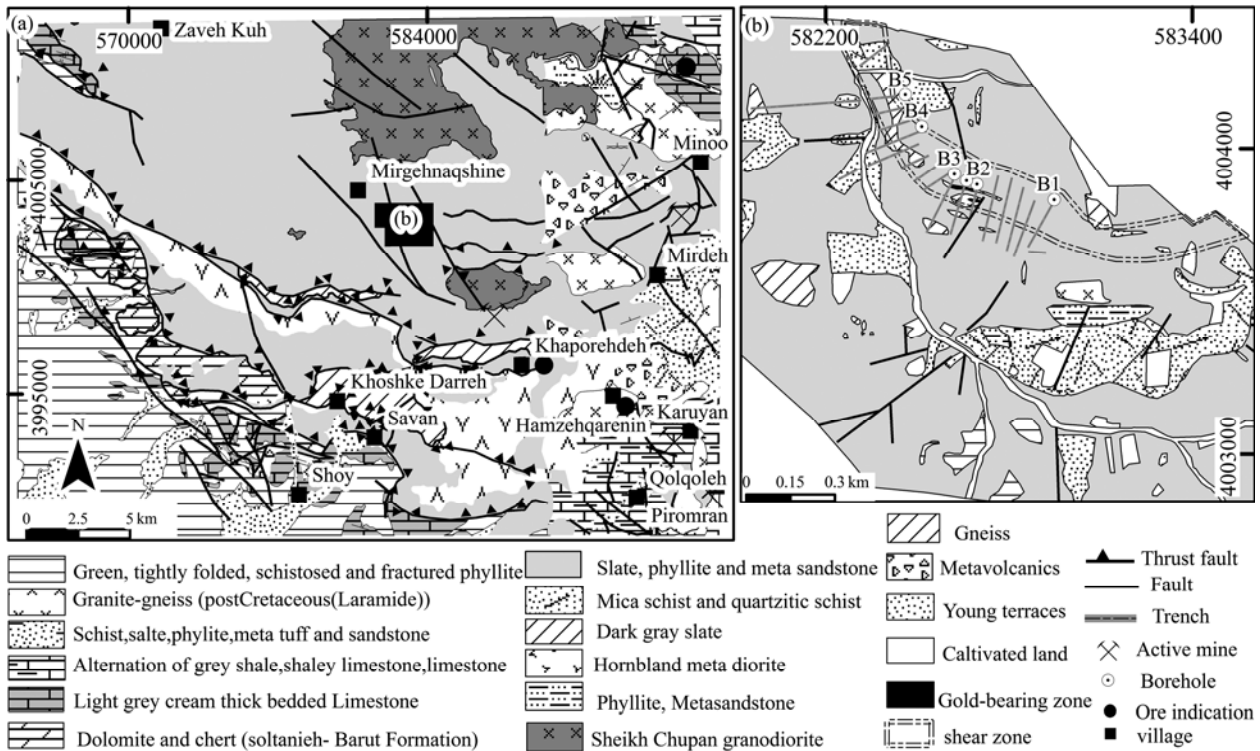


Fig. 2. Geological maps of the Mirge-Naqshineh gold district.

(a), Regional geological map modified from GSI (Geological Survey of Iran, Omrani et al., 2003); (b), Local geological map and location of drill holes used in this study.

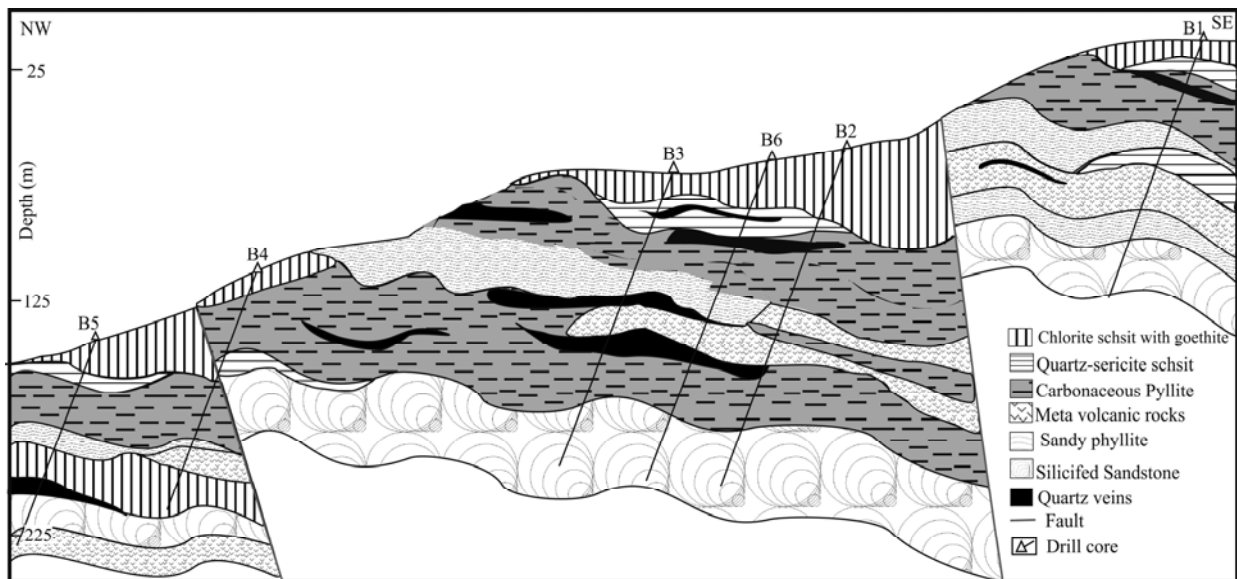


Fig. 3. NW-SE cross section of the B1 to B5 drill holes at the Mirge-Naqshineh, showing volcanic-sedimentary sequence and some of quartz veins.

estimated approximately 2.5 grams per tonne with 65000 tonnes of ore reserve (GIS, 2013).

Planar and linear structures in the study area define three main stages of ductile to brittle deformational events namely D1, D2 and D3 that each of them are included several sub-step: The earliest recognizable deformation (D1) is characterized by a penetrative regional foliation (S1) that is parallel to the bedding (S0) of metasedimentary rocks and accompanied by chloritization and formation of quartz veins parallel to S1. All rock packages and D1 structures in the study area were deformed by a second regional deformational (D2) event.

Based on the structural relationship and petrofabric, three sub-step deformations D2a-D2b-D2c can be recognized in D2 deformation. D2a is the main deformation of D2 that as shown by the presence of S2 foliation, mylonitization, S-C fabric and boudins (Fig. 4a and b). D2b deformation comprises isoclinal folding with NW-SE-trending axial surfaces that have been lead to folding and cutting the auriferous quartz veins (Fig. 4c and d). D2c deformation is detectable with and sercitic foliation that have been overprinted on the S2 foliation

(Fig. 4e). The structures produced by the third step of deformation (D3) are represented by brittle, sub-vertical or steeply dipping, NE-SW or NW-SE trending oblique strike slip or normal faults. This step can be divided into two phases D3a and D3b deformation.

D3a deformation creates low slope extensional fractures which are filled with white quartz-carbonate veins (Fig. 4f). D3b is the youngest stages of deformation in this area include normal and oblique-slip faults, joints, microfractures, microveins and veinlets that are both parallel to and cross-cut mylonitic fabric. The brittle faults commonly include zones of cataclasite and breccia (Fig. 4g). Post-mineralization faulting divides the mineralized area into three distinct blocks that are shown in Fig. 3.

3 Sampling and Analytical Methods

In this investigation, about 150 samples collected from 6 drill core (up to 130 m in depth) and from the surface. Approximately 80 polished blocks and polished thin sections were prepared for ore microscopy and petrography at the Kharazmi University of Iran, and

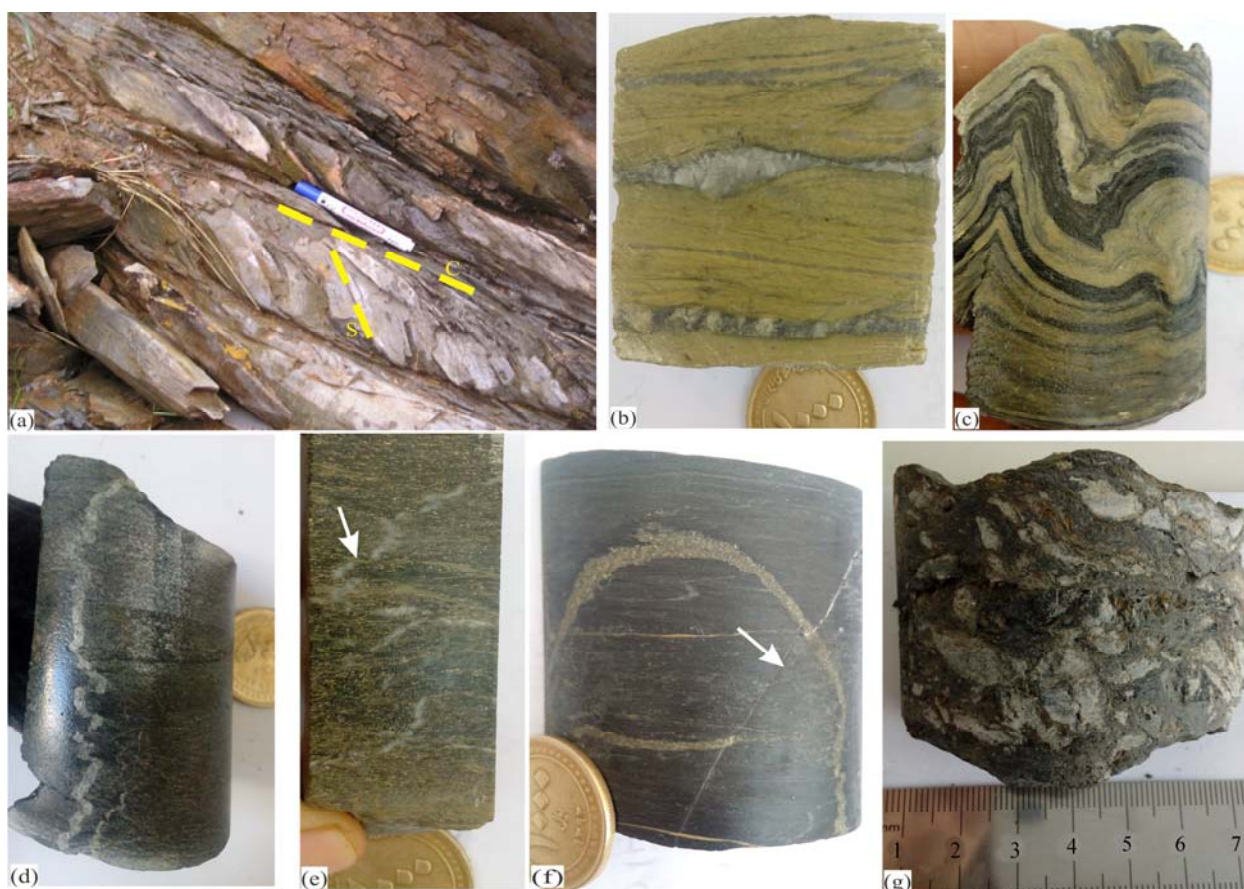


Fig.4. Field and drill core photographs of ductile- brittle deformations in the Mirge-Naqshineh shear zone.

(a), S-C foliation is composed of the shear foliation and mylonite foliation; (b), Boudinated quartz vein; (c), Folded micaschist; (d), Folded vein; (e), Overprinted S2 foliation which cut early quartz vein; (f), Late fracture cutting across quartz-pyrite veinlet in carbonaceous phyllite; (g), Brecciated quartz vein and phyllite associated with a E-W trending fault.

additional scanning electron microscope (SEM) work on these sections was carried out at the Iran Mineral Processing Research Center (IMPRC) laboratory using a LEO 1400 SEM. Backscattered wavelength dispersive electron (BSE) images, energy dispersive X-ray spectroscopy (EDS) and electron microprobe analysis (EPMA) using CAMECA SX100 electron microprobe data were acquired at the IMPRC.

4 Alteration and Veins of the Mirge-Naqshineh Area

Sericitisation and silicification are the major hydrothermal alteration in the wallrock metapelites and metavolcanics in the Mirge-Naqshineh area, and are spatially closely associated with mineralization. Carbonization and chloritization are distal alteration assemblages. Sericitization is best developed in the meta-andesite and tuff adjacent to ore so that only remained pseudomorph of primary phenocrysts in them (Fig. 5a and b). Sericite occurs as flaky aggregates along the foliation and fissures of mylonite and coexists with other alteration minerals (Fig. 5c). Also, sericitization overprinted the pre-existing alterations; this is indicated by cut the earlier quartz-carbonate veins (Fig. 5d), and an increase in modal

proportions of sericite mineral.

Silicification can be divided into two types: (1) free quartz occurs as cement, disseminations and patches that is well developed in the metapelites specifically in meta sandstone; textural features, such as lobate edges, medium-grained crystals, subgrain formation and presence of undulose extinction (Fig. 5e) are suggestive of dynamic recrystallization according to Passchier and Trouw (2005); (2) pervasive silicification occurs as quartz vein and veinlets, stockworks and bands in the wall rocks and orebodies, these veins, veinlets, stockworks and bands are 0.2 to several centimeters wide (Fig. 6); quartz is often intergrown with sericite and pyrite. Pressure solution is pervasive within the Mirge-Naqshineh shear zone and pyrite crystals with quartz pressure shadows are common in mylonite in the shear zone (Fig. 5f). According to Van de Kamp (2008), voluminous silica-rich solutions could be released during intense pressure solution to form quartz veins.

There are three types of structurally controlled veins: Type I veins are bedding-parallel laminated quartz-rich veins with thickness of less than 1 mm to several centimeters that occur with sulphide minerals such as pyrite, arsenopyrite and chalcopyrite. These veins are consisting of gray quartz and dark-colored selvage

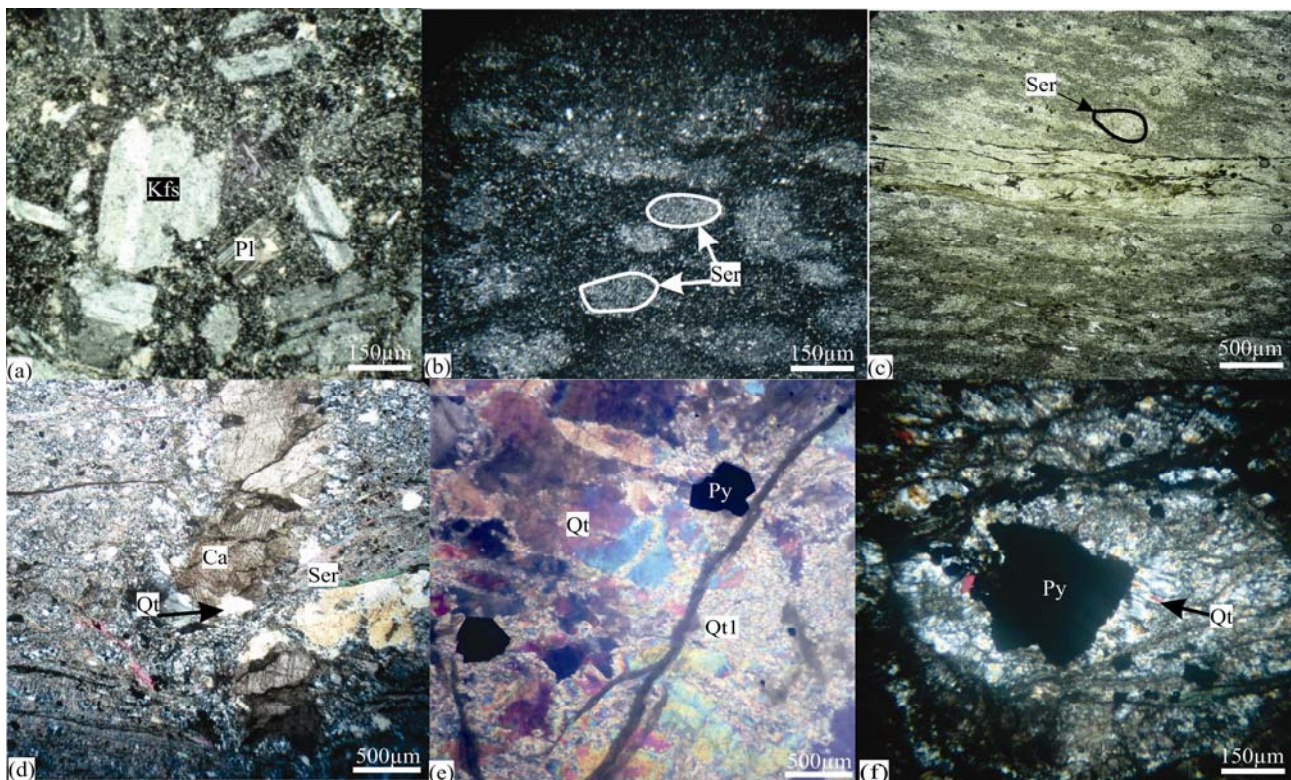


Fig. 5. Photomicrographs showing typical alteration assemblages and host rocks associated with the mineralization.

(a), Unaltered andesitic porphyry with numerous feldspar phenocrysts in surface samples; (b), Sericite pseudomorph of primary phenocrysts in the altered metavolcanic rocks (probably andesite); (c), Aggregates of flaky sericite that extend along foliation and fissures of mylonite; (d), Overprinted sericitic alteration cutting the quartz-carbonate vein; (e), Recrystallized quartz grains (Qt1) associated with pyrite; (f), Pressure shadows of quartz around pyrite. Py – pyrite; Kfs – K-feldspar; Pl – plagioclase; Ser – sericite; Qt – quartz; Ca – carbonate. All photomicrographs in XPL except for (c) in PPL.

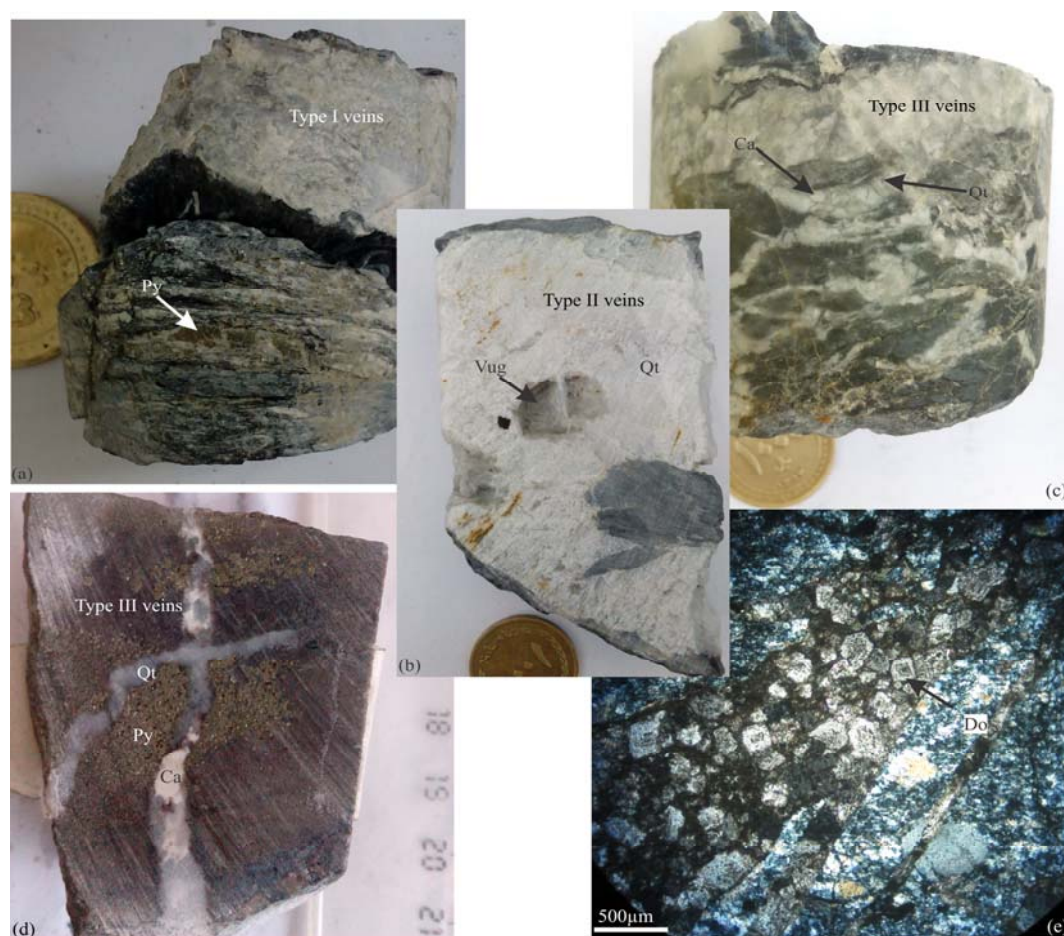


Fig. 6. Photographs of drill-core samples and thin section showing the vein paragenesis in the Mirge-Naqshineh. (a), Bedding-parallel laminated quartz vein in the carbonaceous phyllite (type I); (b), Angular wall-rock inclusions (phyllite) and vug within type II quartz vein; (c–d), Type III quartz-carbonate veins filling fractures; (e), late, dolomite veinlets filling fractures with rhombs and zoned dolomite.

(chlorite, sericite, graphite) (Fig. 6a). It seems that these veins have been created during the D1 deformation, and then boudinaged in D2 deformation (Fig. 4b).

Type II veins are stockworks of white quartz vein and veinlets with a thickness of 1 mm to several centimeters, which also contains vuggy quartz and some pyrite, chalcopyrite and pyrrhotite minerals. Folding with horizontal axial plane is the main deformation in type II veins that represent simultaneous occurrence with D2 deformation. Angular wall-rock inclusions within quartz vein such breccia structures gradually merge into heavily veined wallrock adjacent to the fault zones (Fig. 6b).

Type III veins are late, stockwork microfractures, microveins and extension veins filled with translucent to milky quartz with amounts of calcite-siderite or dolomite (>10% of the veins) (Fig. 6c and d). This vein generation crosscuts type I and II veins and all stages of hydrothermal alteration, and formed during D3a deformation, then cut and displaced during D3b deformation (Fig. 4f). In some cases, the last step fractures (D3b) filled with dolomite rhombs with inclusion-rich cores (Fig. 6e). Sulfides

generally occupy less than 20 vol.% of the mineralized veins. It should be noted that type I and II veins mainly developed in the schistose rocks as well as sericite schist.

5 Ore Mineralogy

Microscopic studies show that the majority of the ore related phases coexist with pyrite in the Mirge-Naqshineh area. Pyrite is the principal sulfide phase (>90% of total sulfides), that occurs in several generations, designated as Py1 to Py6, are identified based on their texture, morphology and interpreted paragenesis.

Py1 are anhedral grains up to 50 µm across with porous texture filled by quartz and sericite and disseminated to form aggregates along bedding planes in the black phyllite and sandstone, with individual grains (Fig. 7a). Py2 displays euhedral to subhedral crystals, coarse grained up to 100 µm, and develops homogeneous grains disseminated in host rocks (Fig. 7b), or overgrows Py1 (Fig. 7a). Abundant inclusions in Py2 consist of sphalerite, pyrrhotite, chalcopyrite, galena and electrum (Fig. 8d).

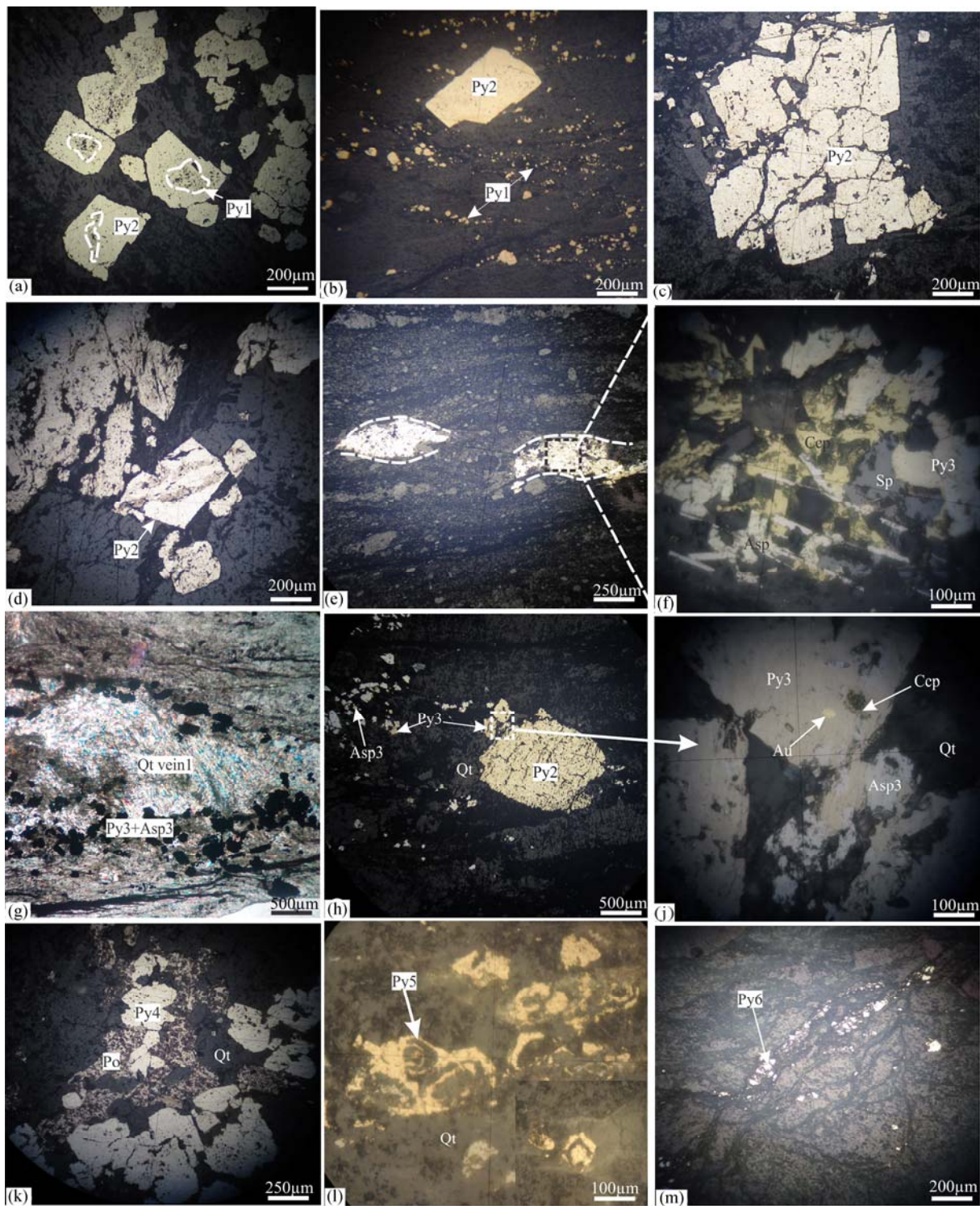


Fig. 7. Photomicrograph (all in reflected light except (g) in transmitted light, crossed nicols) of pyrite types at Mirge-Naqshine. (a), Porous Py1 is overgrown by homogeneous Py2; (b), Disseminated euhedral, Pyrite 2 and anhedral fine grained Py1 aligned parallel to cleavage; (c), Py2 cataclasite in a shear zone; (d), Effect of entered fluid on Py2 showing corrosion and porous texture; (e), Py3 in boudinaged type I quartz vein in the host carbonaceous phyllite; (f), Close up view of (e) Py3 associated with sulfide minerals; (g), Concentration of Py3 and arsenopyrite at margin of type I quartz vein; (h), Py3, arsenopyrite and quartz in pressure shadow around Py2; (j), close up view of gold and chalcopyrite inclusions in Py3 (Note: g, h and j are in the host meta-volcanic); (k), Py4 in type II quartz vein associated with spongy pyrrhotite; (l), Py5 with skeletal texture; (m), late stage pyrite (Py6) filling fissures in host rocks. Asp – arsenopyrite; Ccp – chalcopyrite; Sp – sphalerite; Au – gold; Po – pyrrhotite.

Furthermore, Py2 was commonly fractured during brittle deformation (Fig. 7c) and quartz fibers developed in pressure shadows on edges of it during ductile shearing

(Fig. 5f, 7h). This type of pyrite accounts for more than 70% of the total sulfide minerals among hydrothermal stages. Sometimes fluid entering along with subsequent

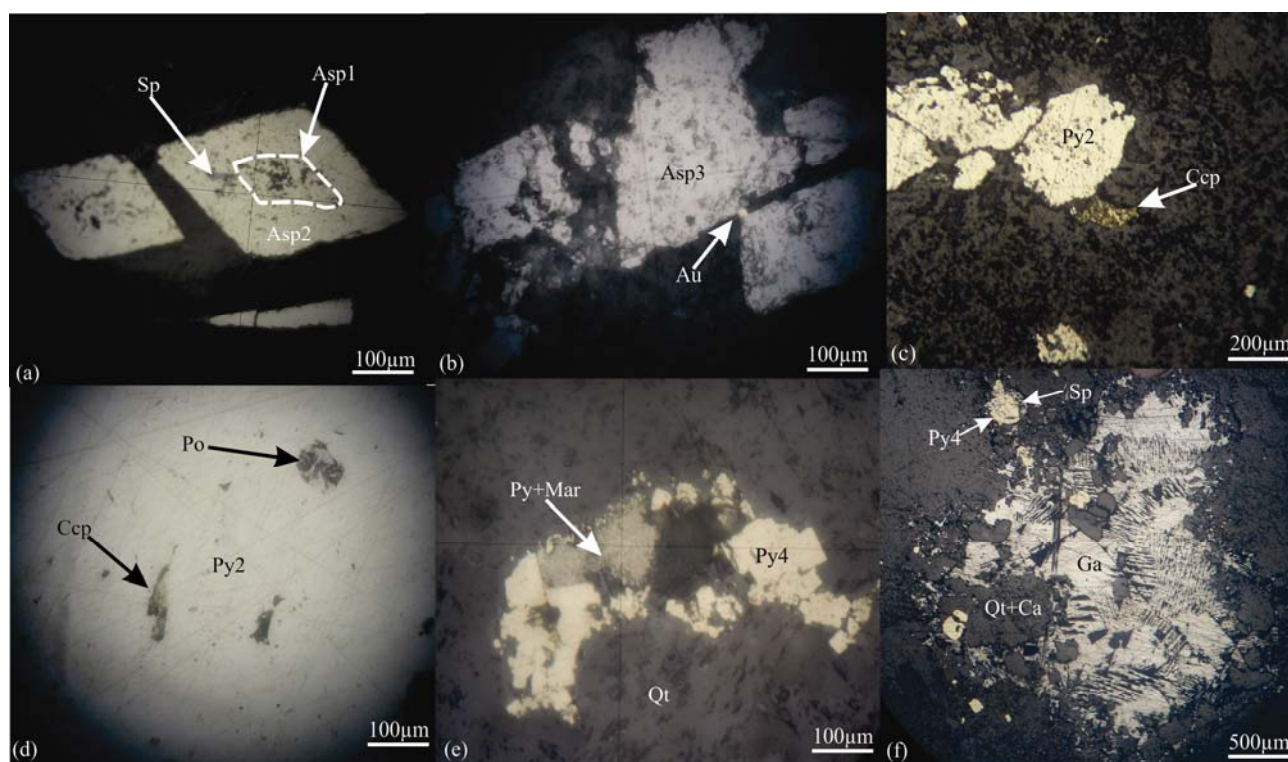


Fig. 8. Reflected light photomicrograph of ore minerals from the Mirge-Naqshineh.

(a), Porous arsenopyrite (Asp1) is overgrown by euhedral and rhombic arsenopyrite (Asp2) with inclusion of sphalerite; (b), Gold particle between columnar arsenopyrites (Asp3) grains; (c), Chalcopyrite and pyrrhotite as inclusions in Py2 matrix; (d), Chalcopyrite and pyrrhotite in Py2 matrix; (e), Marcasite and pyrite with bird's-eye texture after pyrrhotite in quartz vein; (f), Intergrowth of galena, sphalerite and pyrite in quartz-carbonate vein. Mar – marcasite; Ga – galena.

deformation affected on pyrite and lead to corrosion and created pores in Py2 that have filled with gangue minerals (Fig. 7d).

Py3 occurs as euhedral to subhedral crystals and coexists with columnar arsenopyrite, sphalerite and chalcopyrite in the type I quartz vein and veinlets that boudinaged in ductile deformation (Fig. 7e, f). This type often is visible in carbonaceous phyllite but its equivalent in volcanic rocks that are strongly sericitic is euhedral and fine grained pyrite, coexist with rhombus to columnar arsenopyrite and inclusion of gold (Fig. 7g, h, j). Pyrite and arsenopyrite show particular concentration at vein margins, around wall-rock and along slaty laminae in laminated veins (Fig. 7g), also are found in pressure shadows (Fig. 7h).

The fourth pyrite (Py4) consists of euhedral to subhedral pyrite associated with variable amounts of spongy pyrrhotite in the type II quartz veins and veinlets (Fig. 7k). Py5 displays fine grained (10 to 100 μm) pyrite with skeletal texture that is found only along overprinted sericitic foliation in highly altered metavolcanic rocks (Fig. 7l); rapidly quenched of the hydrothermal fluid produces sponge-like textures, often with skeletal mineral grains (Pracejus, 2015). Py6 is formed in late stage and filled the micro fractures; it is fine to medium grained (Fig. 7m).

Arsenopyrite displays columnar, triangular or rhombic crystals ranging from 50 to 200 μm . At least three generations of arsenopyrite can be detected in the Mirge-Naqshineh, one is located in the core of rhombic arsenopyrite with porous texture filled by quartz and muscovite (Asp1; Fig. 8a), and is paragenetically associated with Py1; the other (Asp2) has euhedral crystals often with rhombic shaped cross sections varying from 100 μm to 0.5 mm, or overgrows on Asp1 and is poor of inclusion (Fig. 8a). Asp2 is typically associated with Py2; the last arsenopyrite (Asp3) is columnar shaped coexist with Py3 and gold in type I quartz veins (Fig. 7h, j; Fig. 8b). Chalcopyrite in the form of individual grains disseminated in host rocks and quartz veins (Fig. 8c) as well as has formed inclusion in pyrite 2 and 3 (Fig. 8d).

Pyrrhotite grains or replacement relics of it are found to be included in pyrite porphyroblasts (Fig. 8d), but no pyrite inclusions can be seen inside it, indicating that these pyrite porphyroblasts were formed later than pyrrhotite. Fine-grained pyrite and marcasite have replaced pyrrhotite and appear with bird's-eye texture growing out from coarse-grained pyrite in stockwork quartz veins (Fig. 8e).

Sphalerite occurs as inclusions in pyrite (Py2) and arsenopyrite (Fig. 8a), in addition disseminated along laminations in interbedded sandstone. It is also found associated with chalcopyrite and galena in quartz veinlets.

Galena is found in stockwork quartz carbonate veins associated with Py2, Py6 and sphalerite (Fig. 8f).

Gold mineralization is associated with pyrite, arsenopyrite and galena in quartz veins. Fine particles (10–70 μm) of it exist as subhedral to anhedral inclusions in Py3 (Fig. 7j); also free grains (100 μm) of gold occur along the boundary of arsenopyrite in extensional and lens-like type I quartz veins in the sericitic meta-volcanic rocks (Fig. 8b). SEM-EDS and BSE reveals the presence of electrum and Au-bearing galena in the form of inclusions (10–40 μm long) within the Py2 (Fig. 9a, b).

In addition to, P, REE and U bearing minerals such as monazite, xenotime and apatite were identified by SEM-EDS. Monazite intergrowths commonly located toward sulfide margins as anhedral grains in late stage of filling fractures (Fig. 9c), also appears as randomly dispersed grains in the gangue material. Xenotime-(Y) exists in much lower concentrations in comparison to monazite and apatite (trace amounts). Goethite is present as supergene product of pyrite as red-brown iron hydroxide (Fig. 9d), which decrease downward through the drill cores. Inclusions of gold and marcasite can be seen in highly weathered pyrites (Fig. 9e). Chalcopyrite replaced by covellite in the rim under supergene conditions (Fig. 9f). The main gangue minerals in the Mirge-Naqshineh gold district are quartz, sericite, calcite, chlorite, ankerite,

dolomite, K-feldspar and plagioclase.

6 Minerals Chemistry

Based on the EPMA data of the sulfide minerals (Table 1), almost all generations of pyrite have minor amount of As. The Py4 coexisting with pyrrhotite in quartz vein is free of arsenic, but pyrrhotite contains small amount of it (0.07wt%), (Table 1). The Py3 has the largest amount of arsenic (9.41 wt%). Negative correlation between As and S (Fig. 10a), which have been considered as substitution of As^{-1} for S in the pyrite structure (Fleet and Mumin, 1997; Reich et al., 2005; Deditius et al., 2008), exists in the Mirge-Naqshineh.

Yan et al. (2014) define areas for various types of gold deposits from (Fe+S)-As characteristics of their pyrite. In Mirge-Naqshineh, most of the (Fe+S)-As plots are present in the range of volcanic to metamorphic hydrothermal gold deposits (Fig. 10b). Comparing As concentration of arsenopyrites, Asp3 has higher content of As (41.34wt% to 43.38wt%; Table 1), whereas Asp2 has lower content of it (34wt% to 37 wt%). On the contrary, the Fe (34.15wt% to 35.79wt%) and S (19.75wt% to 29.47wt%) concentrations of arsenopyrite are greater than the standard molecular formula (Fe: 34wt%, S: 20wt%). Minor amounts of Au (0.01wt% and 0.1wt%),

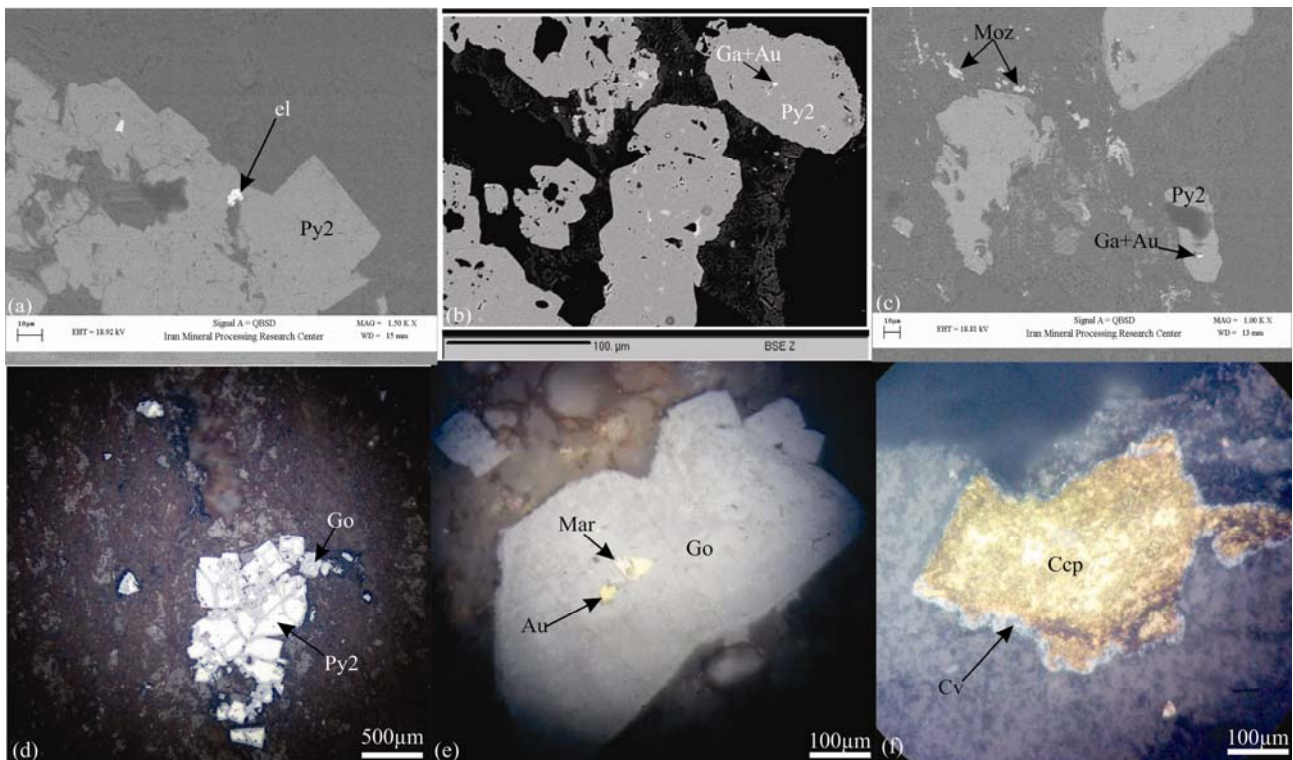


Fig. 9. SEM-EDS, backscattered electron (BSE) image and reflected light photomicrograph of ore minerals from the Mirge-Naqshineh.

(a), Inclusion of Au-bearing galena in Py2; (b), BSE image showing inclusion of electrum in Py2; (c), Unehedral monazite associated with Py2; (d), Goethite reaction rim along cracks of pyrite in supergene weathering; (e), Inclusions of relict gold and marcasite in the pyrite after replacement by goethite; (f), Chalcopyrite altered to covellite in the rim. Go – goethite; Cv – covellite; Moz – monazite; el – electrum.

Table 1 Representative compositions of pyrite, arsenopyrite, sphalerite, pyrrhotite, chalcopyrite and galena in the Mirge-Naqshineh gold district by EPMA (in wt%)

depth (m) sample point	mineral	S	Fe	Cu	Zn	As	Ag	Sb	Te	Au	Pb	Bi	Total	As (at.%)
99.80 M3														
1	Py1	53.34	46.36	<0.01	0.08	0.01	0.09	<0.01	<0.01	<0.01	<0.01	0.01	99.89	
2	Py2	53.34	45.61	0.05	0.11	0.06	<0.01	<0.01	<0.01	0.01	<0.01	<0.01	99.18	
3	Py1	53.31	45.95	0.04	0.01	0.34	0.02	<0.01	<0.01	<0.01	<0.01	<0.01	99.67	
4	Sph	33.95	2.03	<0.01	61.52	0.65	<0.01	<0.01	<0.01	<0.01	<0.01	0.01	98.16	
5	Sph	33.35	3.45	1.08	60.69	<0.01	<0.01	<0.01	<0.01	<0.01	<0.01	<0.01	98.57	
40.20 M5														
1	Py1	53.31	45.66	0.02	0.02	<0.01	<0.01	0.02	<0.01	<0.01	<0.01	<0.01	99.03	
2	Py4	53.2	46.21	<0.01	<0.01	0.29	<0.01	<0.01	0.01	<0.01	<0.01	<0.01	99.71	
3	Ccp	34.4	30.61	34.73	<0.01	<0.01	0.03	<0.01	<0.01	0.03	<0.01	0.16	99.96	
4	Ccp	34.56	30.87	33.73	<0.01	<0.01	0.07	<0.01	<0.01	<0.01	<0.01	<0.01	99.23	
5	Po	39.78	58.80	<0.01	<0.01	0.07	<0.01	0.01	<0.01	<0.01	<0.01	0.22	98.88	
116.70 M1														
1	Py2	52.62	46.85	<0.01	0.03	0.07	<0.01	0.02	<0.01	<0.01	<0.01	<0.01	99.59	
2	Asp2	27.76	35.79	<0.01	<0.01	34.52	<0.01	<0.01	<0.01	0.10	<0.01	<0.01	98.17	23.39
3	Asp2	19.75	34.34	<0.01	<0.01	43.38	<0.01	<0.01	<0.01	0.02	<0.01	<0.01	97.49	31.96
4	Asp1	27.78	34.15	<0.01	0.02	34.69	0.02	<0.01	<0.01	<0.01	<0.01	<0.01	96.66	23.82
5	Asp2	28.38	34.18	0.01	0.03	37.14	<0.01	<0.01	0.02	0.01	<0.01	<0.01	99.77	24.84
6	Asp1	29.47	35.48	0.06	0.03	35.76	0.09	<0.01	<0.01	<0.01	<0.01	<0.01	100.89	23.44
7	Ccp	34.7	30.61	33.83	<0.01	<0.01	<0.01	<0.01	<0.01	0.10	<0.01	0.13	99.37	
8	Po	38.88	59.83	0.010	<0.01	0.05	<0.01	<0.01	<0.01	<0.01	<0.01	<0.01	98.77	
44.40 M4														
1	Ga	12.4	<0.01	<0.01	0.02	<0.01	0.06	0.05	<0.01	<0.01	86.65	<0.01	99.18	
2	Ga	12.56	<0.01	<0.01	<0.01	0.32	0.03	0.08	0.01	<0.01	86.57	<0.01	99.57	
23.20 M2														
1	Py3	46.82	41.70	0.79	0.09	9.41	<0.01	<0.01	<0.01	0.76	<0.01	<0.01	99.57	
2	Py3	52.36	47.05	0.01	<0.01	0.47	<0.01	0.01	<0.01	0.20	<0.01	<0.01	100.1	
3	Asp3	22.95	35.65	<0.01	<0.01	41.35	<0.01	<0.01	<0.01	0.02	<0.01	<0.01	99.97	28.91
4	Asp3	22.66	36.56	<0.01	0.03	39.62	<0.01	0.01	<0.01	0.15	<0.01	<0.01	99.03	27.93
30 M6														
1	Py2	51.48	47.61	<0.01	0.01	0.13	<0.01	<0.01	<0.01	0.03	<0.01	<0.01	99.26	
2	Py2	51.76	47.32	0.02	0.05	0.11	<0.01	<0.01	<0.01	0.01	<0.01	<0.01	99.27	
3	Py2	52.02	47.71	<0.01	0.02	0.14	0.01	<0.01	<0.01	0.02	<0.01	<0.01	99.92	
4	Py1	51.49	47.64	0.02	0.03	0.09	0.01	0.01	<0.01	<0.01	<0.01	<0.01	99.29	

Note: the minimum detection limit is 0.01wt%.

respectively), Cu, Ag, and Te are detected in both Apy2 and Apy3 (Table 1).

Comparison EPMA data between inclusion of sphalerite, chalcopyrite and pyrrhotite within pyrite with disseminated particles of them indicate that, unlike sphalerite disseminated in quartz vein, there is no arsenic in inclusion of sphalerite and Fe, Cu concentrations is higher (3.45wt% Fe; 1.08wt% Cu; Table 1). Craig et al. (1984) suggested that the average Fe content of sphalerite is controlled by coexisting sulfide minerals, primarily as these minerals buffer the fS_2 conditions of the system during precipitation. Copper contents of sphalerite increase with the elevation of temperatures (>400°C), but are reduced significantly at low temperatures (Wang et al., 2003).

Minor amounts of Au, Bi and Ag are present in chalcopyrites, although Ag generally detected in the disseminated type in host rocks and chalcopyrites associated with type I vein are host for Au. Both disseminated pyrrhotite in host rock and pyrrhotite associated with quartz veins have minor amounts of As (0.05wt% and 0.07wt%), but Bi and Sb only have been apparent in pyrrhotite associated with veins. Invisible gold

is found in detectable amounts (100 to 1000 ppm) in arsenian pyrite, arsenopyrite, chalcopyrite and galena. The arsenian pyrite (Py3) with more As (9.41wt%) has higher contents of Au (7000 ppm) specifically related to type I veins. Au can replace Fe/As sites within the lattice of the arsenian pyrite possibly by coupled substitution mechanism (Tauson, 1999; Mishra et al., 2001).

7 Discussion on Metallogenic Evolution, Consideration of Transport and Precipitation of Gold

Based on mineralogy, texture and mineral chemistry studies arsenian pyrites associated with arsenopyrite in type I quartz veins are the main host for gold mineralization at the Mirge-Naqshineh district and mineralization could be summarized into three stages (Fig. 11). In early stage gold mineralization started simultaneously with D1 deformation and precipitation of arsenian pyrite (Py2), electrum and arsenopyrite (Asp1, 2) then, in main stage reaches the highest concentration (gold nanoparticle) in Py3 associated with type I quartz veins, Asp3 and sericitic alteration during D2 deformation.

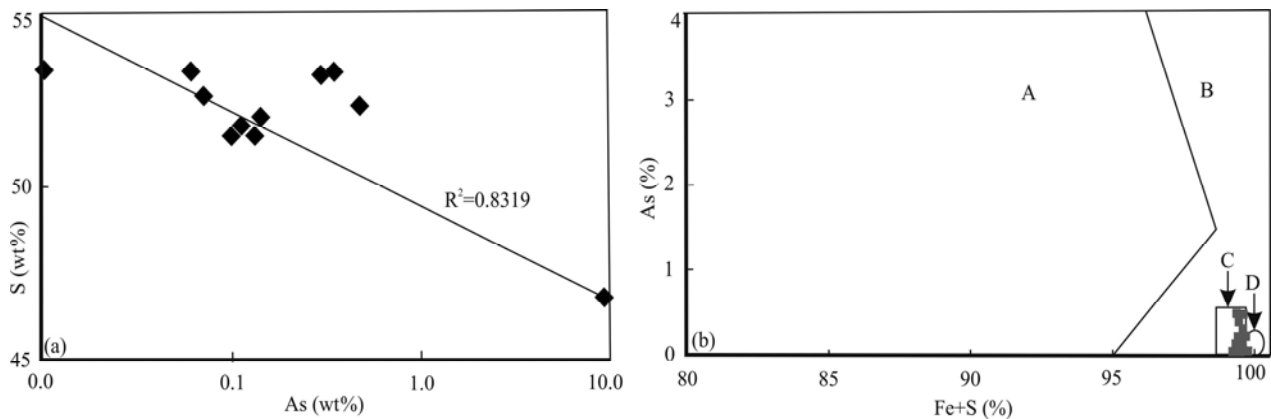


Fig. 10. As, S and Fe relationship in arsenian pyrite of the Mirge-Naqshineh gold district based on the EMPA data. (a), As vs. S variation diagram of arsenian pyrite; (b), the (Fe+S)-As characteristics of arsenian pyrite. Reference fields for A, Carlin-type gold deposits; B, Magmatic hydrothermal gold deposits; C, Volcanic hydrothermal gold deposits; D, Metamorphic hydrothermal gold deposits are from Yan et al. (2014).

Deformation Stages	D1		D2		D3	
Alteration	Early stage		Main stage		Late stage	
Sericite alteration	[Bar]		[Bar]		[Bar]	
Silicification	[Bar]		Q VeinI	Q VeinII	Q VeinIII	
Carbonate alteration	[Bar]		[Bar]		[Bar]	
Chlorite alteration	[Bar]		[Bar]		[Bar]	
Mineral	[Bar]		[Bar]		[Bar]	
Pyrite1	[Bar]		[Bar]		[Bar]	
Pyrite2	[Bar]		[Bar]		[Bar]	
Pyrite3	[Bar]		[Bar]		[Bar]	
Pyrite4	[Bar]		[Bar]		[Bar]	
Pyrite5	[Bar]		[Bar]		[Bar]	
Pyrite6	[Bar]		[Bar]		[Bar]	
Arsenopyrite1	[Bar]		[Bar]		[Bar]	
Arsenopyrite2	[Bar]		[Bar]		[Bar]	
Arsenopyrite3	[Bar]		[Bar]		[Bar]	
Sphalerite	[Bar]		[Bar]		[Bar]	
Chalcopyrite	[Bar]		[Bar]		[Bar]	
Pyrrhotite	[Bar]		[Bar]		[Bar]	
Galena	[Bar]		[Bar]		[Bar]	
Gold	[Bar]		[Bar]		[Bar]	
Electrum	[Bar]		[Bar]		[Bar]	
Monazite	[Bar]		[Bar]		[Bar]	
Covellite	[Bar]		[Bar]		[Bar]	
Goethite	[Bar]		[Bar]		[Bar]	

Fig. 11. Alteration, vein and ore paragenetic sequence for Mirge-Naqshineh.

Based on the As atomic percent in arsenopyrite (Table 1; Fig. 12a), the ore forming temperature of sulfide mineral orebodies without gold particles was 150°C to 180°C and 240°C to 300°C in nanoparticle gold-bearing veins (Kretschmar and Scott, 1976; Sharp et al., 1985). According to chemical modeling by Mernagh and Bierlein (2008), vein mineral and alteration assemblages can reveal the ore forming conditions. This mineral assemblages in the Mirge-Naqshineh gold district and in relationship with type I quartz veins (Fig. 13a) suggest that fluid acidity and redox state has been approximately 4 to 4.5 and reduced

respectively, under 280 to 300°C and 1 kbar condition (Fig. 13c) and that gold would be transported mainly as $\text{Au}(\text{HS})_2^-$ (Fig. 13b).

The solubility of gold depends on pressure, temperature, pH, redox, and concentrations of ligands, such as sulfur, chloride and organic matter, in the hydrothermal fluids (e.g., Stefansson and Seward 2004). Gold precipitation from hydrothermal fluids would be induced by (1) cooling; (2) interaction between ore fluids and country rocks; (3) decreasing $f\text{O}_2$; (4) phase separation in response to a pressure decrease; (5) mixing with another fluid with

different compositions; and (6) interaction with arsenian pyrite (Mernagh and Bierlein, 2008; Wang and Zhu, 2015). Cooling was probably not very important mechanism for gold precipitation in the Mirge-Naqshineh gold district, because at temperatures $<350^{\circ}\text{C}$ steep thermal gradients were unlikely.

According to mineralogical evidence we can only emphasize on arsenian pyrite and interaction fluids-rocks in deposition of gold in the Mirge-Naqshineh. The important role of arsenian pyrite during gold mineralization has been proposed by many studies (Deditius et al., 2014; Wang and Zhu, 2015). The close paragenesis relationship between arsenian pyrite (Py2 and Py3) and gold (Fig. 7j), together with the significant amounts of Au, As in the Py3 (Fig. 12b), both suggest that gold precipitation is undoubtedly related to the crystallization of arsenian pyrite.

The substitution of As^{1-} for S^{1-} in arsenian pyrite facilitates the incorporation of other trace elements, especially invisible Au, due to large amounts of defects in the pyrite structure caused by As substitution (Cook and Chryssoulis, 1990; Fleet and Mumin, 1997; Deditius et al., 2008) and the maximum amount of Au that can be incorporated into pyrite is mainly a function of As concentration (Reich et al., 2005).

In the Au-As plot, (Fig. 12b; following work by Reich et al., 2005), multi-stage hydrothermal pyrites from the Mirge-Naqshineh gold district indeed contain invisible gold as nanoparticles and solid solution. Note that the invisible gold mainly transformed from a solid solution in Py2 to gold nanoparticles in Py3, which implies that conditions of gold mineralization changed from undersaturated to saturate.

It is interesting to note that nanoparticle of gold only occurs within intense sericitic altered volcanic host rocks (andesite and tuff) but this form of gold not occurred within meta-sedimentary rocks. In other words,

hydrothermal fluid has been saturated of gold in type I quartz veins within volcanic rocks whereas is not reached to the extent of saturation within sandstone and phyllite in the Mirge-Naqshineh gold district. The effect of source rock compositions in some of orogenic gold deposits has been considered by researchers (Mernagh and Bierlein, 2008; Pratt, 2016).

Based on alteration assemblage of the host rocks at 300°C in the study area (Fig. 13d) initially quartz + arsenopyrite + muscovite may have precipitated at low rock/fluid ratios near the vein then followed by calcite at intermediate rock/fluid ratios before evolving into the assemblage quartz-calcite-dolomite-chlorite more distal to the vein. Fluid pH and redox state ($f\text{O}_2$) have reached to higher amount in distal alteration (Fig. 13f).

The late stage followed by brittle deformation and formation of type II and III veins. Phase stability relationships in different stage veins also can be estimated using $\log f\text{O}_2$ vs. pH diagram (Fig. 14). Type II vein mainly consists quartz and sulfide minerals (chalcopyrite, pyrrhotite and Py4), which based on EPMA data (Table 1) negligible contents of As, Au within Py4 and absence of arsenopyrite, indicate that compared to the type I vein, the hydrothermal fluids have lower $f\text{O}_2$ in this vein type (Fig. 14). The quartz + carbonate veins (type III) with minor amounts of sulfide minerals (galena, sphalerite, and pyrite) represent more $f\text{O}_2$ compared with other veins. The presence of goethite in the rim of Py2 and covellite in the rim of chalcopyrite suggest marked supergene alteration in the study area.

8 Conclusions

Gold mineralization in the Mirge-Naqshineh district has been result of activity a ductile-brittle shear zone. Based on paragenetic and crosscutting relationship between veins and minerals, have been identified three stages of ore-

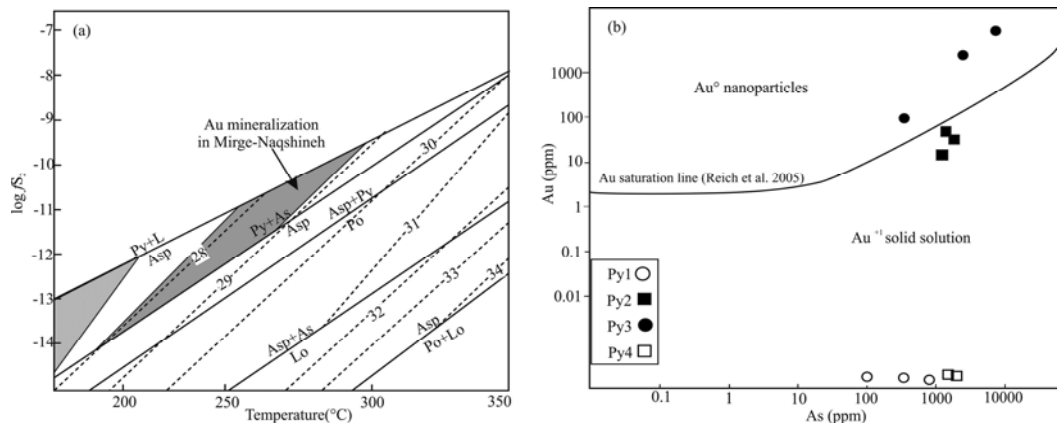


Fig. 12. (a), Formation temperature of arsenopyrite in the Mirge-Naqshineh gold district based on the As atomic percent of arsenopyrite by EPMA (modified by Kretschmar and Scott, 1976; Sharp et al., 1985); (b), Au-As plot showing EMPA analyses of arsenian pyrite (after Reich et al., 2005), indicating that significant invisible gold concentrates in Py3 as nanoparticles and as solid solution in other generation of arsenian pyrite.

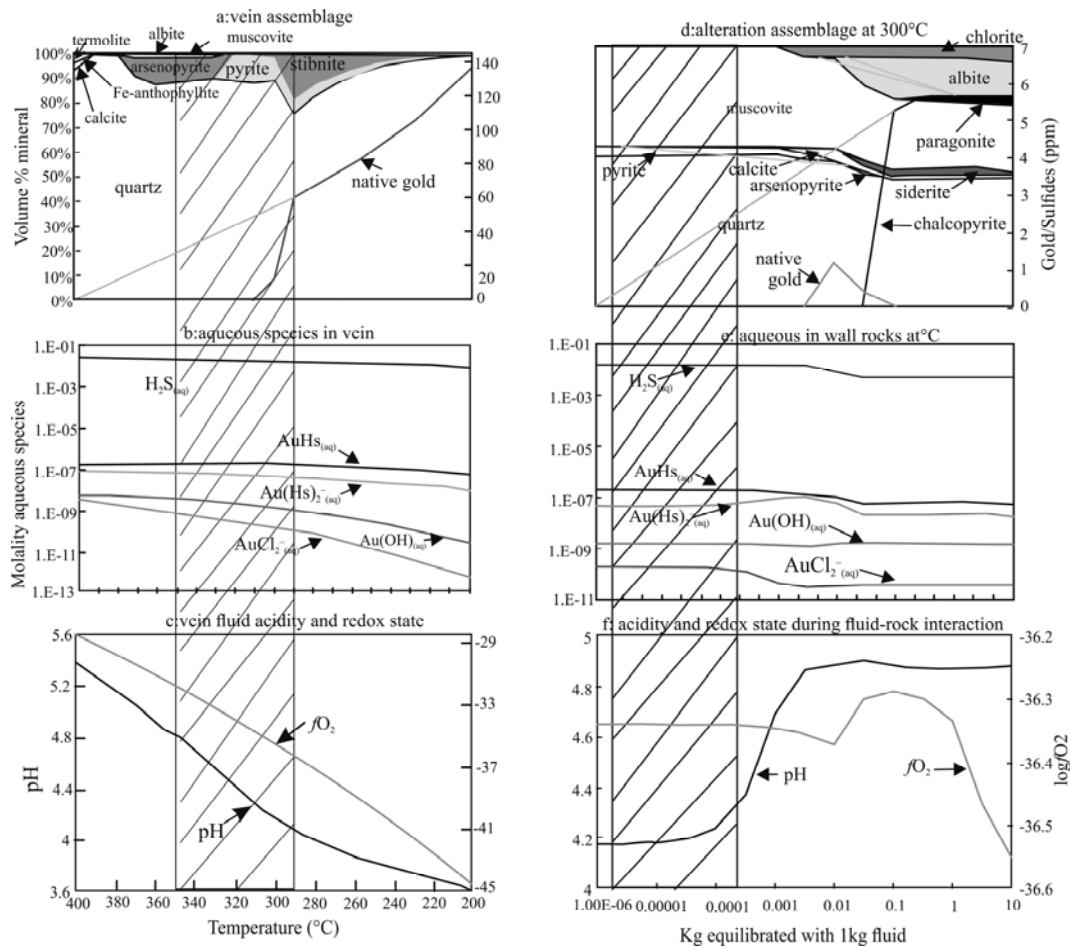


Fig. 13. Chemical modeling of processes of gold deposition at various temperatures from 400°C to 200°C that typically encountered in major orogenic gold deposits from Mernagh and Bierlein (2008). Shaded area showing type I veins of the Mirge-Naqshineh district. The diagrams show minerals predicted to precipitate.

(a), In the vein; (b), The composition of the fluids in the fracture with respect to chosen indicator species; (c), Acidity and *f*O₂ oxidation state of the vein fluid; (d), The predicted alteration assemblage of the host rocks due to fluid-rock interaction at 300°C; (e), The composition of the fluids during fluid rock interaction at 300°C; (f), Acidity and oxidation state of the fluid during fluid-rock interaction.

forming process. Stage II associated with parallel-bedding quartz veins and arsenian pyrite represent the main stage of gold mineralization.

Among the various generations of arsenian pyrite, Py3 has the highest amount of As and Au that existed as gold inclusion. The mineral chemistry of pyrite shows that the Mirge-Naqshineh gold district is a volcanic-metamorphic hydrothermal deposit. Au migrated mainly as Au(HS)₂⁻ complex in hydrothermal fluid and precipitated as a result of fluid-wall rock interaction and changes in pH and *f*O₂ conditions with temperature range 200°–350°C, that accompanied by quartz veins and sericitic alteration.

The source rock composition (interlayers of volcanic rocks) and precipitation of arsenian pyrite provide more favorable conditions for gold concentration. This condition suggest that the ductile deformation (especially in depth) is led to pressure solution and release of hydrothermal fluids then is formed the electrum inclusions in Py2. With the progress of the deformation primary Au in Py2 was consequently released and concentrated as

microscopic inclusions of Au within arsenian Py3 in gold-bearing quartz veins. With the dominance of brittle deformation, environmental conditions have gone towards more oxidation and galena, sphalerite, pyrite, calcite and quartz precipitated within fractures as carbonate-quartz veins.

Acknowledgements

This research is supported by Urmia University and IMIDRO (Iranian Mines and Mining Industries Development and Renovation Organization). Special thanks go for both and unknown reviewer improved my paper quality as well as for Acta Geologica Senica of considering my paper for publication. The authors also wish to thank the Geological Survey of Iran for the permission to sampling of drill cores.

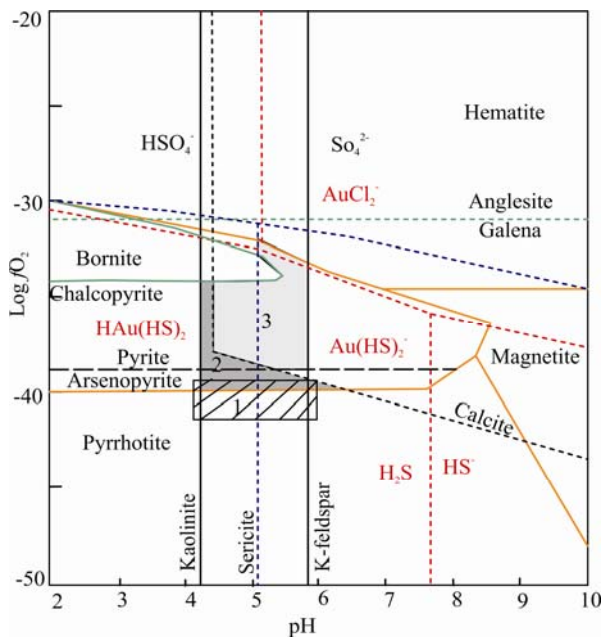


Fig. 14. Log $f(\text{O}_2)$ vs. pH diagram, showing approximate conditions of main and late stages fluid relative to mineral stability in Fe-Cu-O-S system at 260°C (Liu et al., 2016).

The orange and black solid lines represent boundaries of Fe-Cu-O-S minerals, and kaolinite, sericite, and K-feldspar equilibrium, respectively; the black dashed line represents the limit of calcite (Dai and Liu, 1994; Zhang and Spry, 1994) and arsenopyrite (Heinrich and Eadington, 1986). The green dashed line represents the boundary of anglesite and galena equilibrium calculated using thermodynamic data from Cooke et al. (1996). The red and blue dashed lines represent the predominance fields of $\text{Au}(\text{HS})_2^-$, $\text{HAu}(\text{HS})_2^-$, and AuCl_2^- , and aqueous sulfur-bearing species (Hayashi and Ohmoto, 1991; Cooke et al., 1996). The shaded area represents the estimated conditions for type II veins (1), type III veins (3) in late stage and type I veins in main stage (2) sulfide mineralization.

edited by Liu Xinzhu

References

- Agangi, A., Hofmann, A., and Wohlgemuth-Ueberwasser, C.C., 2013. Pyrite zoning as a record of mineralization in the Ventersdorp Contact Reef, Witwatersrand Basin, South Africa. *Economic Geol.*, 108(6): 1243–1272.
- Agard, P., Omrani, J., Jolivet, L., and Mouthereau, F., 2005. Convergence history across Zagros (Iran): constraints from collisional and earlier deformation. *Intl. J. Earth Sci.*, 94(3): 401–419.
- Agard, P., Omrani, J., Jolivet, L., Whitechurch, H., Vrielynck, B., Spakman, W., Monie, P., Meyer, B., and Wortel, R., 2011. Zagros orogeny: a subduction-dominated process. *Geol. Magazine*, 148: 692–725.
- Alavi, M., 1994. Tectonics of the Zagros orogenic belt of Iran: new data and interpretations. *Tectonophysics*, 229: 211–238.
- Aliyari, F., 2006. Mineralogy, geochemistry and fabrics of gold mineralization in ductile to brittle shear zones of the Qolqoleh deposit, southwest of Saqez, Iran. *MSc thesis, Tarbiat Modares University, Iran* (in Persian): 250.
- Aliyari, F., Rastad, E., and Mohajjel, M., 2012. Gold deposits in the Sanandaj-Sirjan zone orogenic gold deposits or intrusion related gold systems. *Res. Geol.*, 62(3): 296–315.
- Baharifar, A.A., Moein Vaziri, H., Bellon, B., and Pique, A., 2004. The crystalline complexes of Hamadan (Sanandaj-Sirjan zone, western Iran): metasedimentary Mesozoic sequences affected by Late Cretaceous tectono-metamorphic and plutonic events. *Comptes Rendus Geosci.*, 336(16): 1443–1452.
- Berberian, M., 1995. Master blind thrust faults hidden under the Zagros folds: active basement tectonics and surface morphotectonics. *Tectonophysics*, 241: 193–224.
- Berberian, M., and King, G.C., 1981. Towards a paleogeography and tectonics evolution of Iran. *Canadian J. Earth Sci.*, 18: 210–265.
- Cooke, D.R., McPhail, D.C., and Bloom, M.S., 1996. Epithermal gold mineralization, Acupan, Baguio district, Philippines: geology, mineralization, alteration, and the thermochemical environment of ore deposition. *Economic Geol.*, 91(2): 243–272.
- Cook, N.J., and Chryssoulis, S.L., 1990. Concentrations of “invisible gold” in the common sulfide minerals. *Canadian Mineral.*, 28: 1–16.
- Cook, N.J., Ciobanu, C.L., Meria, D., Silcock, D., and Wade, B., 2013. Arsenopyrite-Pyrite Association in an Orogenic Gold Ore: Tracing Mineralization History from Textures and Trace Elements. *Economic Geol.*, 108(6): 1273–1283.
- Craig, J.R., Ljokjell, P., and Vokes, F.M., 1984. Sphalerite compositional variations in sulfide ores of the Norwegian Caledonides. *Economic Geol.*, 79(7): 1727–1735.
- Dai, S.B. and Liu, L.D., 1994. Recent development of the study of physico-chemical conditions during gold mineralization. *Journal of Precambrian Metamorphic Geol.*, 3: 65–73 (in Chinese with English abstract).
- Deditius, A.P., Reich, M., Kesler, S.E., Utsunomiya, S., Chryssoulis, S.L., Walshe, J., and Ewing, R.C., 2014. The coupled geochemistry of Au and As in pyrite from hydrothermal ore deposits. *Geochim. Cosmochim. Acta*, 140: 644–670.
- Deditius, A.P., Utsunomiya, S., Renock, D., Ewing, R.C., Ramana, C.V., Becker, U., and Kesler, S.E., 2008. A proposed new type of arsenian pyrite: composition, nanostructure and geological significance. *Geochim. Cosmochim. Acta*, 72: 2919–2933.
- Eftekharnajad, J., 1981. Tectonic division of Iran with respect to sedimentary basins. *J. Iranian Petrol. Soc.*, 82: 19–28 (in Persian).
- Eftekharnajad, J., 1973. The Mahabad Quadrangle map (scale 1:250,000). *Geol. Survey Iran*, Tehran, Iran.
- Fleet, M.E., and Mumin, A.H., 1997. Gold-bearing arsenian pyrite and marcasite and arsenopyrite from Carlin Trend gold deposits and laboratory synthesis. *American Mineral.*, 82: 182–193.
- Ghasemi, A., and Talbot, C.J., 2006. A new tectonic scenario for the Sanandaj-Sirjan Zone (Iran). *J. Asian Earth Sci.*, 26: 683–693.
- Ghorbani, M., 2013. The Economic Geology of Iran: Mineral Deposits and Natural Resources. Springer Geology, 581.
- Hassanzadeh, J., Stockli, D.F., Horton, B.K., Axen, G.J., Stockli, L.D., Grove, M., Schmitt, A.K., and Walker, J.D., 2008. U-Pb zircon geochronology of late Neoproterozoic-Early Cambrian granitoids in Iran: Implications for paleogeography, magmatism, and exhumation history of Iranian basement. *Tectonophysics*, 451: 71–96.
- Hayashi, K.I., and Ohmoto, H., 1991. Solubility of gold in NaCl- and H₂S-bearing aqueous solutions at 250–350°C. *Geochim. Cosmochim. Acta*, 55(8): 2111–2126.

- Heidari, S.M., 2004. Mineralogy, geochemistry and fabrics of gold mineralization in ductile shear zones of Kervian deposit, southwest of Saqez, Iran. *MSc Thesis, Tarbiat Modares University, Iran* (in Persian with English abstract).
- Heinrich, C.A., and Eadington, P.J., 1986. Thermodynamic predictions of the hydrothermal chemistry of arsenic, and their significance for the paragenetic sequence of some cassiterite-arsenopyrite-base metal sulphide deposits. *Economic Geol.*, 81(3): 511–529.
- Kretschmar, U., and Scott, S.D., 1976. Phase relations involving arsenopyrite in the system Fe-As-S and their application. *Canadian Mineral.*, 14: 364–382.
- Liu, C.H., Liu, J.J., Carranza, E.J.M., Yang, L.B., Wang, J.P., Zhai D., Wang, Y.H., Wu, J., and Dai H.Z., 2016. Geological and geochemical constraints on the genesis of the Huachanggou gold deposit, western Qinling region, Central China. *Ore Geol. Rev.*, 73: 354–373.
- McQuarrie, N., 2004. Crustal scale geometry of the Zagros fold-thrust belt, Iran. *J. Struct. Geol.*, 26(3): 519–535.
- Mernagh, T.P., and Bierlein, F.P., 2008. Transport and Precipitation of Gold in Phanerozoic Metamorphic Terranes from Chemical Modeling of Fluid-Rock Interaction. *Economic Geol.*, 103: 1613–1640.
- Mishra, T., Jose, B., Deepa, K.K., Sreehari, S.M.S., and Venkatesh, A.S., 2001. Auriferous mineralization in the Sakoli Group, Central India, with particular reference to sulfide-bound gold. *Applied Earth Sci.*, Transactions of the Institutions of Mining and Metallurgy: Section B, 110(2): 103–109.
- Mohajjel, M., and Fergusson, C.L., 2000. Dextral transpression in Late Cretaceous continental collision, Sanandaj-Sirjan Zone, western Iran. *J. Structural Geol.*, 22: 1125–1139.
- Mohajjel, M., Fergusson, C.L., and Sahandi, M.R., 2003. Cretaceous-Tertiary convergence and continental collision, Sanandaj-Sirjan Zone, western Iran. *J. Asian Earth Sci.*, 21: 397–412.
- Nie, X., Shen, J., Liu H., Du, B., Wang, S., Li, J., Xu, L., and Wang, R., 2017. Geochemistry of pyrite from the Gangcha gold deposit, West Qinling Orogen, China: Implications for ore genesis. *Acta Geologica Sinica* (English Edition), 91(6): 2164–2179.
- Nourian Ramsheh, Z., Mao, J., Yazdi, M., Xiang, J., Rasa, I., and Masoudi, F., 2014. Gold Distribution in Pyrite of the Senjedeh Gold Deposit, Muteh Mining District, NW of Iran. *ACTA GEOLOGICA SINICA* (English Edition), 88(z2):829–830.
- Omrani, J., Agard, P., Whitechurch, H., Benoit, M., Prouteau, G., and Jolivet, L., 2008. Arc magmatism and subduction history beneath the Zagros Mountains, Iran: a new report of adakites and geodynamic consequences. *Lithos*, 106: 380–398.
- Omrani, J., and Khabbaznia, A.R., 2003. Geological map of Alut (scale 1:100,000). *Geol. Survey Iran*, Tehran.
- Passchier, C.W., and Trouw, R.A., 2005. *Microtectonics* (2nd ed.), Berlin: Springer, 289.
- Pracejus, H.B., 2015. *The ore minerals under the microscope: An Optical Guide: Atlases in Geoscience 3*. Netherlands: Elsevier, 1101.
- Pratt, W., 2016. A classification of styles of orogenic (shear zone) gold mineralization, with examples from Scandinavia. *Applied Earth Sci.*, 125: 94.
- Reich, M., Kesler, S.E., Utsunomiya, S., Palenik, C.S., Chryssoulis, S.L., and Ewing, R.C., 2005. Solubility of gold in arsenian pyrite. *Geochim. Cosmochimica Acta*, 69: 2781–2796.
- Sarkarinejad, K., and Azizi, A., 2008. Slip partitioning and inclined dextral transpression along the Zagros Thrust System, Iran. *J. Structural Geol.*, 30: 116–136.
- Sharp, Z.D., Essene, E.J., and Kelly, W.C., 1985. A re-examination of the arsenopyrite geothermometer: pressure considerations and applications to natural assemblages. *Canadian Mineral.*, 23: 517–534.
- Stefansson, A., and Seward, T.M., 2004. Gold (I) complexing in aqueous sulphide solutions to 500°C at 500 bar. *Geochim. Cosmochim. Acta*, 68(20): 4121–4143.
- Tajeddin, H., Drri, M., and Niroomand, S., 2004. Gold mineralization in Barika sheared zone (East of Sardasht, western Azarbaijan). 22nd Geoscience Symposium, *Geol. Survey Iran* (in Persian).
- Tauson, V.L., 1999. Gold solubility in the common gold-bearing minerals: experimental evaluation and application to pyrite. *European J. Mineral.*, 11: 937–947.
- Thomas, H.V., Large, R.R., Bull, S.W., Maslennikov, V., Berry, R.F., Feraser, R.F., Froud, S., and Moye, R., 2011. Pyrite and Pyrrhotite Textures and Composition in Sediments, Laminated Quartz Veins, and Reefs at Bendigo Gold Mine, Australia: Insights for Ore Genesis. *Economic Geol.*, 106(1): 1–31.
- Van de Kamp, P. C., 2008. Smectite-Illite-Muscovite Transformations, Quartz Dissolution, and Silica Release in Shales. *Clays Clay Mineral.*, 56: 66–81.
- Wang, L., and Zhu, Y., 2015. Multi-stage pyrite and hydrothermal mineral assemblage of the Hatu gold district (west Junggar, Xinjiang, NW China): Implications for metallogenic evolution. *Ore Geol. Rev.*, 69: 243–267.
- Wang, Y.W., Wang, J.B., and Wang, L.J., 2003. An Unusual Texture: Skeletal Sphalerite in Pyrite from Dajing Tin-polymetallic Deposit, China. *Res. Geol.*, 53: 67–72.
- Yan, Y., Zhang, N., Li, S., and Li, Y., 2014. Mineral chemistry and isotope geochemistry of pyrite from the Heilangou gold deposit, Jiaodong Peninsula, Eastern China. *Geosci. Frontiers*, 5: 205–213.
- Zhang, H., Cai, Y., Ni, P., and Zhang, Y., 2017. The Occurrence Mechanism of Gold in Pyrite from the Qiucun Gold Deposit in Fujian Province, China. *ACTA GEOLOGICA SINICA* (English Edition), (z1):61–62.
- Zhang, X., and Spry, P.G., 1994. Petrological, mineralogical, fluid inclusion and stable isotope studies of the Gies gold silver telluride deposit, Judith Mountains, Montana. *Economic Geol.*, 89: 602–627.

About the first author

Golale ASGHARI, Ph.D. student at Geology Department at Urmia university, Urmia, Iran; born in Kurdistan province, on September 19, 1984. She attended in Bu-Ali Sina University and earned a Bachelor of Science degree in geology in 2007; carried out graduate studies (MSc) at Tehran University, in geology in 2009. During graduate studies she worked in several small companies as an intern for the Geological Survey of Iran. Golale is an author on 9 articles in national journals and conference proceedings. This paper is from her Ph.D. thesis under supervision of Professor Samad Alipour.